Tin dioxide from first principles: Quasiparticle electronic states and optical properties

A. Schleife,[1,2,3] J. B. Varley,[3] F. Fuchs,[1,2] C. Rödl,[1,2] F. Bechstedt,[1,2] P. Rinke,[2,4] A. Janotti,[4] and C. G. Van de Walle[4]

[1]*Institut für Festkörpertheorie und -optik, Friedrich-Schiller-Universität, Max-Wien-Platz 1, D-07743 Jena, Germany*
[2]*European Theoretical Spectroscopy Facility (ETSF)*
[3]*Department of Physics, University of California, Santa Barbara, California 93106-9530, USA*
[4]*Materials Department, University of California, Santa Barbara, California 93106-5050, USA*

The structural, electronic, and optical properties of the semiconducting oxide SnO_2 are investigated using first-principles calculations. We employ the G_0W_0 formalism based on hybrid-functional calculations to compute the quasiparticle band structure and density of states for which we find good agreement with results from photoemission and two-photon absorption experiments. We also address open questions regarding the band ordering and band symmetries. In a second step we use our electronic structure as a starting point to calculate optical spectra by solving the Bethe-Salpeter equation including the electron-hole interaction. The dielectric tensor is predicted for a wide range of photon energies. Our results resolve the long-standing discrepancy between theory and experiment on the highly anisotropic onsets of absorption. The anisotropy can be explained in terms of dipole-allowed direct transitions in the vicinity of the valence-band maximum without having to invoke lower-lying valence bands.

PACS number(s): 61.66.Fn, 71.15.Qe, 71.20.Ps, 71.35.Cc

I. INTRODUCTION

The wide-band-gap semiconductor SnO_2 has long been a material of interest for both applied and pure research. Tin dioxide has most notably been employed as a transparent conductor, exploiting both the unintentional conductivity and the large degree of transparency.[1,2] While nominally *n* type, recent work has suggested that SnO_2 may be more easily doped *p* type than several other commonly used oxides such as ZnO, indicating that it may be a better choice for light emitters and other optoelectronic devices.[3–6] In order to fully exploit SnO_2 as a semiconductor for such novel applications, knowledge of the electronic structure is of critical importance. Despite the vast experimental and theoretical literature on SnO_2, many discrepancies and unsolved issues remain. These include details of the valence-band (VB) ordering and band symmetries,[7–10] the role of indirect transitions,[9,11,12] and the exciton spectrum.[10,13–15] Although SnO_2 is widely used for its optical properties, its dielectric function is not available in the literature. Experimentally the explored energy range was limited,[16,17] while a theoretical study neglected the impact of excitonic effects.[18]

SnO_2 is known to crystallize in the rutile structure with space group $P4_2/mnm$ or D_{4h}^{14} (*SG*136) under ambient conditions.[19,20] The fundamental gap is direct but the corresponding dipole transitions are symmetry forbidden. This was originally suggested based on group-theoretical arguments on the orbital character of the band edges.[13,14,21] Accordingly, the respective onsets in single-photon optical-absorption experiments are weak.[21–25] Despite the relatively small absorption coefficients, these experiments have revealed the polarization dependence of the onsets. While the transitions are dipole forbidden in single-photon absorption, they are allowed in two-photon absorption, and the measured value of 3.6 eV[10,26] is now widely accepted as the band gap of SnO_2. We note that neither optical absorption nor two-photon absorption probe the *fundamental gap* as given by the difference between the ionization potential and the electron affinity. Instead, they provide the *optical gap*, i.e., the excitation energy of the first accessible exciton state. If the exciton derives from the band edges, the optical and the fundamental gap differ by the exciton binding energy, which is on the order of 30 meV in SnO_2.[10,21,25] A measurement of the fundamental gap by direct and inverse photoemission spectroscopy (PES and IPES, respectively) has, to our knowledge, not been reported yet. It is also unlikely that the combination of PES and IPES would reach the accuracy to resolve a 30-meV difference in the two band gaps.

The selection rules for dipole transitions can be derived using the symmetry of the states and group theory. Several experimental studies have converged on a symmetry assignment of the VB maximum (VBM) at Γ as Γ_3^+ (in the irreducible representation notation of Koster *et al.*[27]), through analysis of the quadrupole transition to the $1s$ exciton.[26,28] The agreement of a VBM of Γ_3^+ also settled the symmetry assignment of the Sn s-derived conduction-band minimum (CBM) as Γ_1^+, as suggested by experimental arguments[13,14,29] and calculations.[9,11]

The experimental results largely agree that the lowest dipole-allowed direct (direct-allowed) transition features a strong polarization anisotropy, but the origin of this transition is heavily debated. Experimental[10] as well as theoretical[7–9,11] reports are plagued by inconsistencies in the ordering and relative energies of the lower-lying VB states. Naga-sawa and Shionoya reported an allowed transition value of 3.75 eV for light polarized perpendicular to the tetragonal *c* axis ($E \perp c$), which they associated with a VB of symmetry Γ_5^- lying 0.15 to 0.20 eV below the VBM.[15] For light polarized parallel to *c* ($E \parallel c$), the absorption spectra exhibit a diffuse edge approximately 0.4 eV above the fundamental edge,[22–24] lacking the fine excitonic structure of the absorption spectra for perpendicular light polarization.[10,13,14,24] This feature was assigned to a hypothetical valence band with Γ_2^- symmetry[23,24] lying 0.4 eV below the Γ_3^+ VBM, consistent with their interpretation of direct, symmetry-allowed transitions in the same study.

Several other experiments found no distinct peaks at lower temperatures and a weak temperature dependence in the spectra, suggesting that the absorption onsets were not associated with phonon-assisted transitions.[22–24]

Up until now no theoretical band structure is capable of explaining all experimental facts for SnO_2. The earliest self-consistent calculations for SnO_2, employing the augmented-plane-wave[11] and linearized muffin-tin orbital[9] methods, along with more recent ones in the augmented-spherical-wave[12] method, predicted an indirect gap with the VBM at the R point instead of Γ. Tight-binding calculations by Robertson[8] seemed more consistent with the experimental interpretations of a direct gap and highest-lying VB symmetry assignments, by showing a VB of the suggested symmetry Γ_5^- approximately 0.2 eV below the VBM.[15,22–24] However, the next lower VB in Robertson's calculations was at -0.8 eV, which cannot explain the experimentally observed absorption onsets and interpretations. As expected, calculations within the local-density or generalized gradient approximation (LDA, GGA, respectively) lead to a very strong underestimation of the fundamental band gap.[30,31] Since the simple approach that Thomazi *et al.* applied to incorporate quasiparticle (QP) effects requires knowledge of the experimental band gap, it cannot overcome this deficiency in an *ab initio* manner.[31] Moreover, the fact that many details of the band structure are very sensitive to the theoretical method used, particularly the behavior at the R point of the Brillouin zone (BZ), warrants further attention.

In this paper we show that our theoretical spectroscopy methods are capable of providing a unified picture of the electronic structure and the optical properties of SnO_2 that is consistent with the various experimental observations. More specifically, we present state-of-the-art many-body perturbation theory calculations of the QP band structure based on Hedin's GW approximation.[32–34] Furthermore, we solve the Bethe-Salpeter equation (BSE) for the polarization function to calculate the optical properties, including excitonic and local-field effects (LFE).[33,35,36]

A description of the methodology is given in Sec. II. Following a short review of the atomic structure in Sec. III, the QP and optical properties of SnO_2 are analyzed in detail in Secs. IV and V. Throughout, the computed results are compared with the available experimental data. The paper concludes with a summary of our findings in Sec. VI.

II. COMPUTATIONAL METHODS

In this paper we distinguish between ground- and excited-state properties. The former (e.g., structural properties) are well described in the framework of density-functional theory (DFT).[37,38] All calculations have been performed with the Vienna *ab-initio* Simulation Package (VASP).[39–41] We use the projector-augmented wave (PAW) method[42,43] to model the electron-ion interaction, which allows us to accurately treat even the localized O $2s$- and Sn $4d$-derived states at plane-wave cutoffs of 450 eV. For exchange and correlation (XC) we use the LDA.[44,45] The Brillouin zone is sampled with a $8 \times 8 \times 14$ **k**-point Monkhorst-Pack (MP) mesh[46] which has been shifted to include the Γ point. The relaxed atomic geometries and lattice parameters are obtained by minimizing the total energy.

For the final structures the forces acting on the ions are well below 5 meV/Å.

The excited-state properties are studied by means of many-body perturbation theory (MBPT). For a comparison with photoemission spectra of solids and band structures from angle-resolved photoemission spectroscopy, MBPT within Hedin's GW approach[47] is currently the method of choice.[32–34] We compute the band structure by solving the QP equation with the self-energy $\Sigma = i\hbar GW$, where W is the dynamically screened Coulomb potential and G denotes the single-particle Green's function. In practice, QP energies are usually calculated via the G_0W_0 approach, i.e., within first-order perturbation theory based on an initial electronic structure from Kohn-Sham DFT. However, the DFT-LDA gap of 1.08 eV drastically underestimates the experimental value. DFT-LDA therefore provides a poor starting point in this case, resulting in the G_0W_0 band gap significantly underestimating the experimental gap. An effective way to obtain a suitable initial electronic structure is to remove or significantly reduce the self-interaction error from the ground-state calculation.[34,48–52] In the present work, we use the hybrid XC functional HSE03,[53] which contains a fraction of short-ranged Hartree-Fock exchange. This choice, denoted as HSE03+G_0W_0, has recently been demonstrated to give reliable values for the fundamental gaps and d-band binding energies of typical semiconductors and insulators.[49,51,54] Due to the much higher computational cost of this scheme compared to an ordinary LDA calculation, we decrease the sampling of the BZ to $6 \times 6 \times 10$ Γ-centered MP **k** points, which yields QP energies converged to within 0.1 eV.

In order to compute the macroscopic dielectric function and the absorption spectrum we go beyond the GW approach in MBPT and include the attractive screened electron-hole interaction, as well as an exchange-like term that accounts for LFE, by solving the BSE[35,36] for the polarization function. Both of these effects have proven to be essential for a successful calculation of the macroscopic dielectric function.[35,55,56] Computationally it is, however, very challenging to converge these two terms. Resolving exciton binding energies and features near the absorption edge within the necessary accuracy of several meV requires a fine **k**-point sampling of the center of the BZ.[57] For the calculation of the optical absorption spectrum up to photon energies of more than 20 eV, on the other hand, a large number of conduction bands (CBs) is needed.

To keep the calculations tractable, we sample the BZ using a hybrid **k** mesh with increased density in the vicinity of the BZ center for the low-energy region of the imaginary part of the macroscopic dielectric function. The inclusion of transitions up to photon energies of $\hbar\omega = 20$ eV is accomplished with a reduced **k**-point sampling and an increased number of CBs. Details of this approach are given in Ref. 51. More precisely, we calculate the dielectric function up to 9.95 eV using a hybrid $6 \times 6 \times 10 : 3 \times 3 \times 7 : 14 \times 14 \times 21$ **k** mesh. This nomenclature (cf. Ref. 57) is our shorthand notation for a BZ sampling by a regular $6 \times 6 \times 10$ MP mesh, whose inner $3 \times 3 \times 7$ region is replaced by an $8 \times 8 \times 16$ MP mesh. The density in the inner region is then equal to that of a $14 \times 14 \times 21$ sampling of the entire BZ. For the dielectric function above 9.95 eV we use a regular $6 \times 6 \times 10$ MP mesh. To accelerate the convergence even more we apply a small random shift to all of these **k** meshes to lift potential degeneracies at high-symmetry points
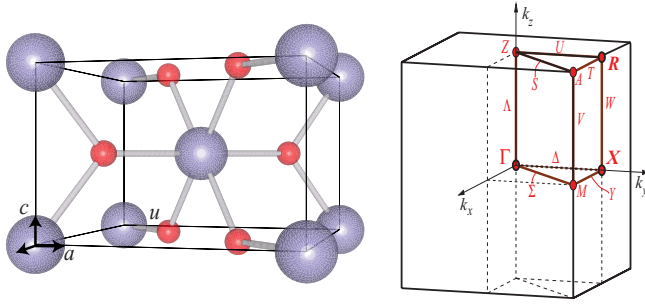
FIG. 1. (Color online) Bonding geometry of the tetragonal unit cell of SnO_2 in the rutile structure with the associated Brillouin zone. The special points R, X, and the zone center Γ are highlighted.

and lines that are inherently present when MP meshes are being used. The screening of the Coulomb potential in the excitonic Hamiltonian is described by a model dielectric function[58] that uses the dielectric constant of $\varepsilon_\infty = 3.62$ that we calculated in the random-phase approximation (RPA).

A common approach to solve the BSE, which is also applied in this work, is to transform the integral equation to an eigenvalue problem for the excitonic electron-hole pair Hamiltonian.[55,59,60] The resulting matrices are large with ranks up to 80 000, despite the adapted BZ sampling technique. Hence it is practically impossible to diagonalize these matrices for a computation of the dielectric function by means of the eigenstates and eigenvalues. Instead, we overcome the cubic scaling of the direct diagonalization by using an efficient time-evolution scheme,[61] which scales quadratically with the rank of the excitonic Hamiltonian, to obtain the dielectric function.

A simplification of the problem is necessary with regard to the electronic structure that the optical calculations are based on. The HSE03+G_0W_0 method is computationally too expensive to generate input for the large number of **k** points and CBs required for converged calculations of the optical properties. For that reason we approximate the HSE03+G_0W_0 results by those of an LDA+U+Δ method,[51,54] i.e., by an LDA+U band structure[62] whose CBs are shifted up rigidly by a scissors shift Δ. We apply the LDA+U approach of Dudarev *et al.*[63] U and Δ are obtained from a comparison to our HSE03+G_0W_0 band structure which leads to a good agreement of the results from both approaches, as illustrated in Sec. IV A.

III. ATOMIC GEOMETRY AND ELASTIC PROPERTIES

In the rutile structure of SnO_2, shown in Fig. 1, each Sn atom is octahedrally coordinated and bonded to six O atoms. The total energy, the cell volume, and the bulk modulus as well as its pressure derivative have been computed using the Murnaghan equation of state[64] to fit the energy versus volume dependence in the vicinity of the equilibrium volume. Table I summarizes the calculated lattice parameters, elastic constants, and the cohesive energy of rutile SnO_2 in comparison to experimental results. The computed lattice constants are in excellent agreement with the experimental values.[19] Remarkable agreement is also found between the calculated internal cell parameter u

TABLE I. Structural parameters, bulk modulus, and cohesive energy for rutile SnO_2 as calculated within DFT-LDA. Experimental values are listed for comparison.

	a (Å)	c (Å)	u	B (GPa)	B'	E_{coh} (eV/f.u.)
This work	4.737	3.200	0.306	200	3.6	−5.83
Expt.	4.737[a]	3.186[a]	0.307[a]	205[a]	7.4[a]	−5.98[b]

[a]Reference 19.
[b]Value cited in Ref. 66.

with values from neutron-diffraction[20] and x-ray-diffraction[19] experiments. Our values for c/a and u agree well with previous hybrid functional[65] and DFT-GGA results,[18] while our a lattice constant turns out to be about 2% smaller than the DFT-GGA value.

The calculated value of the bulk modulus B, also given in Table I, is in very good agreement with the experimental result. Its pressure derivative B', however, differs significantly from the reported experimental value. Given the excellent agreement between computed and measured values for all of the other structural parameters, we suggest that the experimental value may be less accurate in this case. The observed agreement for the cohesive energy is also satisfactory, demonstrating that our ground-state calculations capture the structural properties of SnO_2 with sufficient accuracy to provide a solid foundation for studying the electronic structure.

IV. ELECTRONIC STRUCTURE

A. Quasiparticle band structure

Figure 2 shows the QP band structure and density of states (DOS) of rutile SnO_2 calculated using the HSE03+G_0W_0 and LDA+U+Δ approaches. In addition, the fundamental gap and the d-band binding energy are given in Table II. As stated in the introduction, the lowest exciton transition of 3.56 eV measured in the two-photon absorption experiments by Fröhlich *et al.*[26] is now widely accepted as the band gap of SnO_2. The corresponding fundamental gap is obtained by adding the exciton binding energy of ∼30 meV.[10,21,25] Our
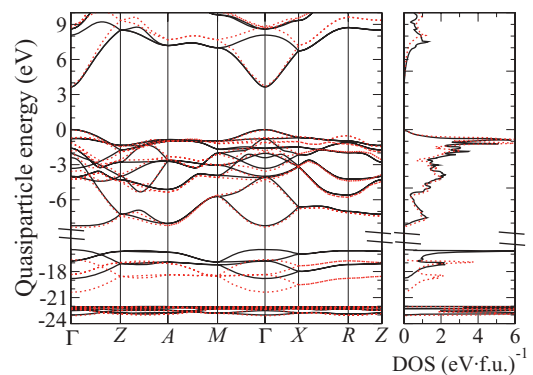

FIG. 2. (Color online) Quasiparticle band structure and density of states of rutile SnO_2 in HSE03+G_0W_0 (dotted red lines) and LDA+U+Δ (solid black lines). The valence-band maximum has been chosen as the common zero of energy.

TABLE II. Quasiparticle gap (E_g), average d-band binding energy (E_d), and effective electron (m_c^*) and hole masses (m_v^*) at Γ of rutile SnO_2 as computed using the HSE03+G_0W_0 approach, shown with the respective experimental values.

	E_g (eV)	E_d (eV)	m_v^* (m_0)		m_c^* (m_0)	
			Γ-X	Γ-Z	Γ-X	Γ-Z
HSE03+G_0W_0	3.65	22.3	1.21	1.47	0.26	0.21
Expt.	3.56[a]	21.5,[b]22.5[c]			0.299[d]	0.234[d]

[a]Reference 26.
[b]Reference 67.
[c]Reference 68.
[d]Reference 69.

calculated HSE03+G_0W_0 gap of 3.65 eV is in very good agreement with the resulting ~3.59 eV.

As alluded to in Sec. II, the LDA+U+Δ band structure (shown as solid black lines in Fig. 2) has been calculated as a basis for the subsequent calculations of the optical properties. The parameters U and Δ were chosen to give the best agreement with the HSE03+G_0W_0 band structure. We fix the U parameter at $U = 4.6$ eV which describes the position of the d-band complex (with respect to the VBM) very well, as can be seen from a comparison to the HSE03+G_0W_0 QP bands. However, we want to note that deviations remain for the O $2s$-derived bands at approximately −18 eV and the upper VBs around Γ. Also the sensitivity of the R point in the BZ to the computational method used is made apparent by the difference in the LDA+U+Δ and the HSE03+G_0W_0 band structures in Fig. 2. In contrast to the HSE03+G_0W_0 results, the indirect gaps at the Z and X points are smaller than the one at R in LDA+U+Δ. The R point is found too low in the LDA+U description, which is interesting and confirms previous reports on the sensitivity of this point to the chosen methodology.[9,11,12] Furthermore, it potentially explains many of the discrepancies and inconsistencies that have plagued calculations of the electronic structure of SnO_2.

While LDA+U improves on the LDA for the fundamental band gap, the value of 1.19 eV still severely underestimates the HSE03+G_0W_0 result. We therefore use $\Delta = 2.46$ eV to rigidly shift the CBs relative to the VBs which leads to an agreement between the gap within the LDA+U+Δ method and the value obtained from HSE03+G_0W_0.

B. Irreducible representations and allowed transitions

In our calculations, the VBM is found at the Γ-point of the BZ and has the Γ_3^+ irreducible representation, consistent with the interpretation of experiments in Refs. 26 and 28. The CBM derives from Sn s states, as originally suggested,[13,22] and is found at the Γ point with symmetry Γ_1^+, also consistent with previous reports both in its irreducible representation and location in the BZ.[7–9,11,13,14,26,29] The relative VB ordering together with the QP energies, the allowed optical transitions, and the respective real-space symmetry of the states at Γ are shown in Fig. 3. Our calculated band structure does not exhibit the conjectured lower-lying VBs approximately 0.2 or 0.4 eV below the VBM.[23,24] Although we observe that the next-lowest VB level *is* a doubly degenerate state with the Γ_5^-
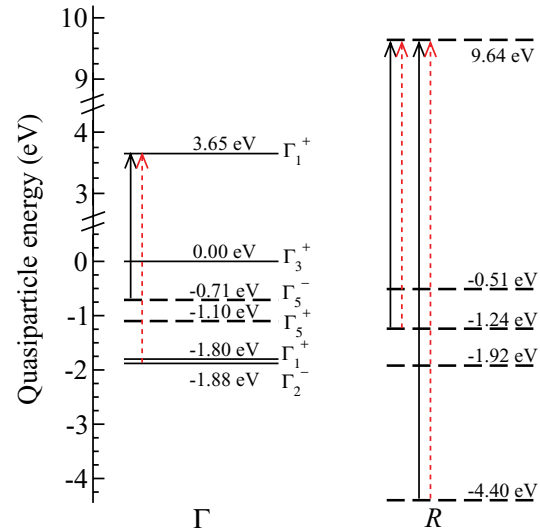

FIG. 3. (Color online) Plot of the HSE03+G_0W_0 quasiparticle eigenvalues together with allowed optical transitions at the Γ and the R points of the Brillouin zone. Dashed lines indicate a twofold degeneracy of the respective level. Solid black (dotted red) arrows show dipole-allowed optical transitions for light polarized perpendicular (parallel) to the c axis of the rutile lattice.

irreducible representation, which is consistent with the same set of experiments,[23,24] it occurs *only* at 0.71 eV below the VBM and thus cannot account for their observations.

In Fig. 3 we have also included the QP energies for the R point together with the corresponding symmetry-allowed optical transitions. Although the 0.51-eV difference between the energy of the topmost VB at Γ and the one at the R point is smaller than the distance of 0.71 eV between the highest two VBs at Γ, we can conclude that the R point does not play a role in the observed absorption, as indirect transitions from the topmost VB at R to the CBM at Γ can support neither a VB at 0.2 nor at 0.4 eV below the VBM.[23,24] In addition, we find that these transitions from the R point to the CBM are also dipole forbidden. This view is supported by temperature-dependent measurements that suggest a minimal contribution from phonon-assisted transitions.[22–24]

It is important to acknowledge that the calculations which are reported here do not take the spin-orbit interaction into account. However, as a test we performed a calculation using the HSE03 XC functional with the spin-orbit interaction included.[70] This allows us to conclude that any shifts in the band positions or splittings of twofold degenerate levels are quite small. More specifically, we found a splitting of the Γ_5^- (Γ_5^+) state of only 25 meV (18 meV), which cannot explain why a band approximately 0.2 or 0.4 eV below the VBM would occur, as suggested in Refs. 23 and 24. In Sec. V we will demonstrate that all experimental results on the absorption edge in SnO_2 can be understood by computing the optical spectrum from first principles.

C. Density of states

Figure 4 shows the HSE03+G_0W_0 DOS plotted alongside an experimental photoemission spectrum by Nagata *et al.*[68] To facilitate comparison with experiment, we introduced
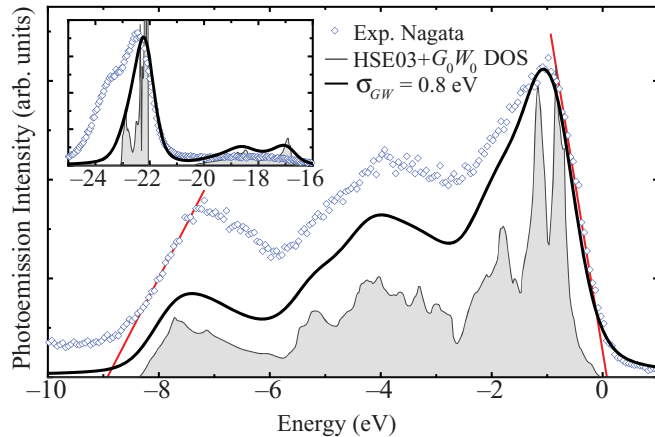
FIG. 4. (Color online) Calculated density of states of rutile SnO$_2$ compared to experimental photoemission spectra. Open circles denote the XPS data by Nagata *et al.* (Ref. [68]). The plot includes the HSE03+G_0W_0 DOS without broadening (gray shaded region), as well as with Gaussian and Lorentzian broadening (FWHM σ = 0.8 eV), as explained in the text. The unbroadened DOS has been scaled by a factor of 0.5 to allow for visual comparison of all features of the spectrum. The zero of energy is chosen at the theoretical VBM, and the red lines indicate band-edge extrapolations. The inset shows the agreement between theory and XPS for the lower-lying VB complex derived from Sn 4d and O 2s states.

broadening in the calculated DOS as follows. To account for the instrumental resolution, we first convolved the calculated DOS with a Gaussian curve of 0.8 eV full width at half maximum (FWHM). We then convolved the resulting curve with a Lorentzian, again with a FWHM of 0.8 eV, to simulate the finite lifetime broadening that is intrinsic to photoemission experiments. The experimental spectra were then aligned with the broadened calculated DOS based on the O 2p and other upper VB peaks, following the practice in previous alignment procedures between theory and experiment.[71–73] Inspection of the projected DOS (not shown) reveals that the group of bands between −6 and 0 eV derives mostly from O 2p and Sn 5p/Sn 4d states, whereas the bands in the region between −8.3 and −6 eV derive from a hybridization between O 2p and Sn 5s states. The topmost VB protrudes from the VB complex only in a small region of the BZ, as Fig. 2 illustrates. Its associated DOS is therefore small and becomes almost indistinguishable from the onset of the first broad peak at −1 eV that derives from the VBs around −0.71 eV (at Γ) and below.

When the theoretical spectra are broadened to match experiment, the peak from the topmost VB is almost completely washed out, which would make a precise experimental identification of the VB edge very difficult in the absence of a proper reference. In our computed spectra, this reference is of course still provided by the VBM, which we set as our zero of energy. By aligning the peak positions of the experimental spectrum of Nagata *et al.*[68] to the broadened HSE03+G_0W_0 DOS, we were able to establish the position of the VBM of the photoemission spectrum. As shown in Fig. 4, the linear extrapolation from the upper peak edge of the experimental data is within 0.07 eV of the theoretical VBM.

Photoemission experiments can provide information about the fundamental gap if the position of the Fermi level (which is used as a reference for the spectra) is known with respect to the band edges. All that is known about the Fermi level in the experiments of Nagata *et al.*[68] is that the SnO$_2$ sample was n type, and therefore the Fermi level is expected to be in the proximity of the CBM. We found that a 3.56-eV shift is necessary to align the theoretical and experimental spectra. Assuming that the experimental Fermi level is at the CBM, the tentative estimate of the band gap in photoemission is therefore ∼3.6 eV. A more accurate determination of the Fermi level in the samples would reduce the uncertainty.

Between approximately −17 eV and −23 eV we find another complex of bands predominantly of Sn 4d and O 2s character (see inset of Fig. 4). Interestingly, our average d-band binding energy of 22.3 eV is in much better agreement with experiment (cf. Table II) than previous reports for d bands in II-VI compounds[34,48,49,74–77] and in group-III nitrides.[34,48,49,75]

The overall bandwidths[67,68] and the relative peak positions and intensities show very good agreement between the HSE03+G_0W_0 results and photoemission spectra. Our value for the bandwidth of the upper band of 8.3 eV falls in between the 9 eV from older ultraviolet photoemission spectroscopy (UPS) results of Gobby and Lapeyre for the (001) surface[78] and the 7.5 eV extrapolated from the tails of the peaks in the more recent UPS measurements of Themlin *et al.* for the (110) surface.[71] The same group also performed x-ray photoemission spectroscopy (XPS) measurements on (110)-oriented SnO$_2$, with an apparent VB width of 10.4 eV in the absence of extrapolations,[67] in better agreement with the apparent width of approximately 9.0 eV from Nagata *et al.* (Fig. 4). Other calculated VB widths of 6.6 eV,[9] 7.5 eV,[12] and 10 eV (Refs. [7] and [8]) are even further away from the accepted value of 9 eV from Gobby and Lapeyre,[78] while other hybrid functional calculations have produced similar results to ours.[65]

D. Effective masses

From parabolic fits to the HSE03+G_0W_0 band structure we derived the effective masses of the highest VB and the lowest CB at the Γ point, along the principal directions Γ-X and Γ-Z. These values are included in Table II. The effective masses for electrons agree reasonably well with the best experimental results as determined by submillimeter cyclotron resonance.[69] We note that the inclusion of QP effects improves the agreement with experiment in comparison to previous results from DFT-GGA (Ref. [18]) and hybrid functionals.[65] The effective hole masses are predictions since they are yet to be measured, but are smaller than previous calculations.[65] However, the effective hole masses are consistent with previous speculations of a $m_v^* > m_0$ based on arguments involving the exciton structure and anisotropy parameters of SnO$_2$ as explained in Ref. [15].

V. OPTICAL PROPERTIES

The origin of the optical spectrum at the absorption onset has been heavily debated ever since the first experiments on SnO$_2$ were published in the 1960s. As phonon-assisted transitions were ruled out by temperature-dependent

measurements,[23,24] dipole-allowed direct transitions (i) from lower-lying VBs or (ii) from the vicinity of the VBM (called "direct-forbidden" transitions in Ref. 14) were proposed as possible explanations for the observed absorption onsets. As discussed in Secs. IV A and IV B, our calculations conclusively show that no lower-lying VBs of the right energy are present at Γ, such that explanation (i) is not viable. As for (ii), on the basis of calculated absorption spectra, we will provide a consistent explanation for the experimental findings in terms of these direct-forbidden transitions that occur just off Γ and are highly polarization dependent. While such transitions were speculated to explain the peculiar absorption behavior in SnO_2,[14] they can be easily misidentified as originating from lower-lying VBs of the appropriate symmetry, explaining why there has been so much confusion in the literature.

A. Dielectric function

Calculating the optical spectrum based on the full QP band structure and including the electron-hole attraction as well as LFE by solving the BSE is currently the state-of-the-art. Due to the large computational cost of calculating QP energies using $HSE03+G_0W_0$, the number of **k** points in the calculation is too small to obtain a converged optical spectrum. The $LDA+U+\Delta$ method allows us to account for QP energies at much lower computational cost and facilitates the convergence of the optical calculations. Since we determine the parameters U and Δ from comparison to the $HSE03+G_0W_0$ band structure, no information from the QP band structure is lost (cf. Sec. IV A).

No experimental spectrum exists for a wide photon-energy range. As a result of the tetragonal crystal structure of rutile SnO_2, only two components of the dielectric tensor are independent, i.e., $\varepsilon_\perp (= \varepsilon_{xx} = \varepsilon_{yy})$ and $\varepsilon_\parallel (= \varepsilon_{zz})$. They can be measured in ordinary ($\varepsilon_\perp$) and extraordinary ($\varepsilon_\parallel$) polarization. In Fig. 5 we compare the optical spectra calculated in the independent QP approximation (IQPA) and the result from
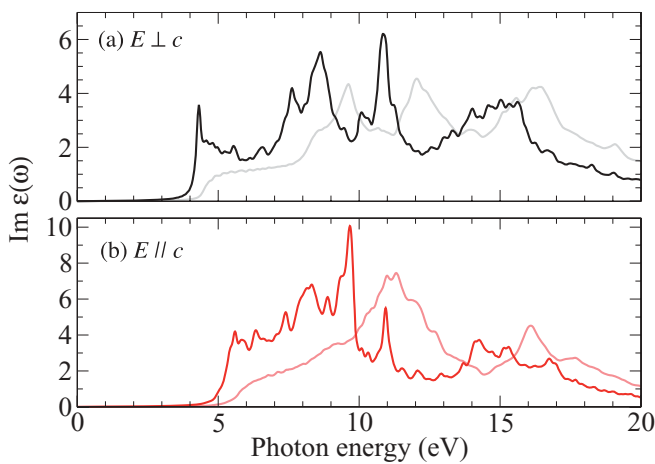

FIG. 5. (Color online) Imaginary part of the dielectric function in the IQPA (gray, light red) and from the solution of the BSE (black, red). We show the results for light polarization perpendicular (a) and parallel (b) to the *c* axis of the rutile crystal structure. The anisotropy in the vicinity of the absorption edge becomes more pronounced when excitonic effects are included.

the BSE approach. We observe a strong influence of the excitonic effects resulting in a significant redshift of the peak positions and a redistribution of oscillator strength toward lower energies. The absorption onset of the BSE curves occurs about 0.9 eV lower in energy compared to the absorption onset of the IQPA curves, for both parallel and perpendicular polarizations.

There is a dramatic difference between the respective energetic positions of the absorption onsets for the two polarization directions (cf. Fig. 5). This anisotropy has been observed experimentally, but only in a fairly narrow energy range near the absorption edge; we will return to this issue below. In contrast, our calculations include photon energies up to 20 eV, and we find that the anisotropy (i.e., $\varepsilon_\perp$ being very different from $\varepsilon_\parallel$) extends over this entire energy range.

B. Exciton binding energies

All dielectric functions and the optical spectra in this paper were obtained by solving the Bethe-Salpeter equation. This approach could in principle also be applied to determine the energy of bound excitons in the QP gap. However, to converge the exciton binding energy very high **k**-point densities are necessary,[57] leading to extreme demands with respect to computing power. Therefore we calculate these binding energies using the solution of a parabolic two-band Wannier-Mott model.[57,79] It has been shown that such an approach agrees very well with BSE values reported in previous studies for similar materials.[57] Moreover, this strategy is justified by the parabolic shape of the lowest CB and the uppermost VB of SnO_2 (cf. band structure in Fig. 2). Using the effective mass values reported in Table II and the RPA screening constant of $\varepsilon_\infty = 3.62$ as calculated in the independent-particle approximation, the two-band model gives exciton binding energies of $E_B = 222$ meV for ordinary (perpendicular) polarization and $E_B = 191$ meV for extraordinary (parallel) polarization. These results substantially overestimate the experimental values of approximately 30 meV.[10,80] The reason for this large overestimation is probably the omission of ionic screening in our first-principles calculations.[57,81]

For SnO_2 the difference between the experimental *static* dielectric constants $\varepsilon_0^\perp = 14$ ($\varepsilon_0^\parallel = 9$) (Ref. 82) and the *electronic* dielectric constants (that take only electronic excitations into account and are sometimes also called high-frequency dielectric constants) $\varepsilon_\infty^\perp = 3.785$ ($\varepsilon_\infty^\parallel = 4.175$) (Ref. 83) is large, which indicates that the electron-lattice coupling is not negligible. The ionic screening should in principle be taken into account in the screened Coulomb interaction in the GW and the BSE approach as well, but no successful calculation has been reported so far and it is not entirely clear how to include the electron-lattice interaction consistently into the parameter-free formalism. We illustrate the large impact of the ionic contribution by employing the average of the experimental *static* dielectric constants,[82] $\varepsilon_0 = (2\varepsilon_0^\perp + \varepsilon_0^\parallel)/3 = 12.3$, in the formula for the binding energy of the Wannier-Mott exciton.[57,79] This leads to values of $E_B = 19$ meV (ordinary polarization) and $E_B = 16$ meV (extraordinary polarization) which are much closer to the experimental results,[10,80] now slightly underestimating them. This indicates that the actual screening in the material is somewhere between ε_0 and ε_∞.
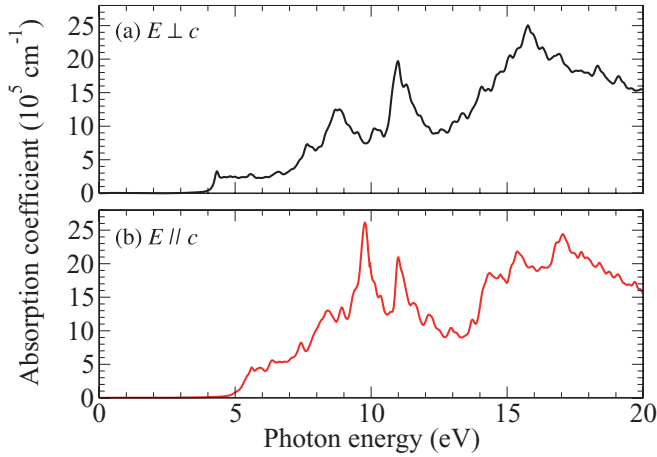
FIG. 6. (Color online) Absorption coefficient calculated from the BSE for perpendicular (a) and parallel (b) light polarization.

At variance with earlier studies, Reimann and Steube[10] observed three separate exciton series in two-photon spectroscopy experiments. The associated transition energies for the lowest exciton in each series differed by 0.05 and 0.1 eV.[10] This would suggest that SnO_2 should have three states at either the VB or CB edge that are of nearly the same energy and effective mass, in clear contradiction to our calculated band structure. We suggest two possible explanations for the discrepancy. First, some of the exciton series in the Reimann experiment could be due to impurity-bound excitons. Second, since Reimann and Steube reported twinning, their SnO_2 samples may have been composed of domains with different strain. Strain can shift the absolute energetic position of the bands, and consequently also the respective exciton series.[84] It is noteworthy that earlier[26] as well as later[80] experiments report only one exciton series.

C. Origin of direct-forbidden transitions

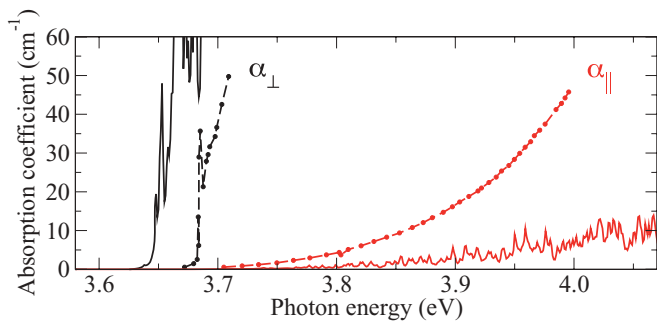In Figs. 6 and 7 we return to the anisotropy of the absorption edge. The experimentally reported absorption coefficients[24]

FIG. 7. (Color online) Absorption coefficient calculated from the BSE for SnO_2 (solid lines) plotted alongside the experimental results at $T = 7$ K (circles) (Ref. 24) for perpendicular (black curves on the left) and parallel (red curves on the right) light polarization. Lorentzian broadening of 0.001 eV has been added to the calculated results to simulate the lifetime and instrumental broadening inherent to experiment. The broadening artifacts below the absorption edge have been subtracted.

lie in the range of 0–100 cm^{-1}, which is several orders of magnitude *lower* than typical absorption coefficients for the onset of allowed transitions in SnO_2 (cf. Fig 6). We will show that this behavior at the absorption edge arises from direct-*allowed* transitions with very small oscillator strengths in the vicinity of the VBM at Γ. In order to investigate this issue we employed an even more refined $6\times6\times10 : 3\times3\times5 : 10\times10\times18 : 3\times3\times5 : 56\times56\times100$ double-hybrid **k** mesh (nomenclature as before, cf. Ref. 57) in reciprocal space. The resolution provided by such a fine mesh allows for studying the absorption in the direct vicinity of the Γ point including the respective polarization dependence provided by the dipole-matrix elements. In contrast to the calculation of the entire spectrum, we chose the screening constant of $\varepsilon_0 = 12.3$ for the highly resolved study of the absorption edge for reasons discussed before. To account for lifetime and instrumental broadening, the absorption coefficients in Fig. 7 have been calculated with a small Lorentzian broadening of 0.001 eV.

The agreement with the experimental curves[24] is reassuring. Both the steep onset of the absorption for perpendicular polarization as well as the slow increase for parallel polarization at slightly higher photon energies is reproduced. Our theoretical curves appear to be shifted to lower energies by approximately 50 meV, which is in line with our error bar of ∼0.1 eV for the underlying QP band structure and approximations we have made for the dielectric constant.

In order to understand the small absolute values of the absorption coefficient around the band edge at 3.65 eV, as well as their polarization dependence, we investigate the optical dipole-matrix elements $|\mathbf{p}|$ (calculated within the longitudinal approximation[85]). We find that all components of $\mathbf{p}$ are zero for transitions between the VBM and the CBM at the zone center. This is consistent with our assignments of the irreducible representations Γ_1^+ (CBM) and Γ_3^+ (VBM) as well as with experiment (e.g., Ref. 26). However, as shown in Fig. 8, the dipole-matrix elements for perpendicular polarization ($|p_\perp|$) grow as soon as we move off the zone center along several directions in the BZ. This rapid increase leads to the increase of the absorption coefficient for perpendicular polarization that we observe in Fig. 7. Nevertheless, these matrix elements remain significantly smaller than those associated with typical dipole-allowed transitions (see, e.g., Ref. 86 for MgO, ZnO,
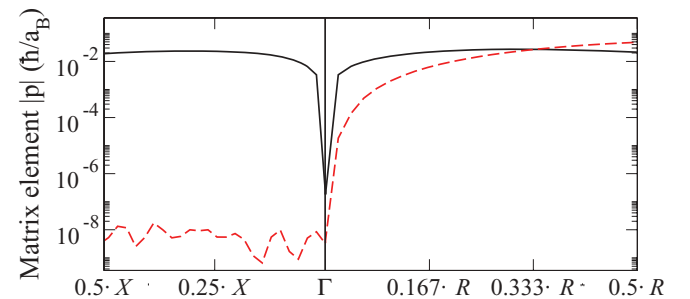

FIG. 8. (Color online) Absolute value of the optical transition-matrix elements (in units of $\hbar/a_B$) along two high-symmetry directions in the Brillouin zone for light polarized perpendicular ($|p_\perp|$, solid black) as well as parallel ($|p_\parallel|$, dashed red) to the tetragonal c axis.

and CdO), explaining the small magnitude of the absorption coefficient.

In contrast, the matrix elements for the parallel polarization $|p_\parallel|$ tend to stay very small when moving off Γ along various high-symmetry directions. The only direction along which we observe an increase of $|p_\parallel|$ is $\Gamma - R$ (cf. Fig. 8). This behavior of the dipole-matrix elements explains our results for both the magnitude and the dichroism of the absorption coefficient, in excellent agreement with experimental observations.[24]

We thus conclude that dipole-allowed direct transitions off Γ (called direct-forbidden transitions in Ref. 14) are the dominant mechanism responsible for the anisotropic absorption onsets, rather than indirect transitions.[24] The weak dependence of the absorption coefficient on temperature further supports the conclusion that the transitions are *not* indirect.[23] Some experimental papers attributed the onsets of absorption for the perpendicular and parallel polarizations to direct-allowed transitions from lower-lying VBs of symmetry Γ_5^- and Γ_2^- at approximately 0.2 eV (Ref. 15) or 0.4 eV (Refs. 22–24) below the VBM. Our calculations clearly show that no such VBs are present in this energy range, and that they are not needed to explain the experimental findings.

Overall, our exhaustive study of the absorption in SnO_2 explains the early temperature- and polarization-dependent experiments of Nagasawa and Shionoya[24] that highlight the weak onset. Figure 5 also shows a strong onset of the imaginary part of the dielectric function at about 4.0 eV, consistent with the observed rise of the absorption coefficient to values of about 10^4–10^5 cm^{-1} (see Fig. 6) in SnO_2 films with low free-carrier concentrations.[87]

VI. SUMMARY AND CONCLUSIONS

We have presented a systematic *ab initio* study of the band structure and optical properties of the semiconducting oxide SnO_2. For the QP band structure, our HSE03+G_0W_0 results give a direct, dipole-forbidden band gap of 3.65 eV, in good agreement with experimental findings. Additional features such as the VB width, binding energy of the Sn 4d states, and anisotropic electron effective masses are also in remarkable agreement with experimental results. For the hole effective masses, which have not yet been experimentally determined, we provide predictions.

For the optical spectrum, we have been able to accurately resolve the absorption onset in the presence of bound electron-hole pairs. This facilitates a direct comparison with experiment and reveals that the difference in the observed gaps for $E \perp c$ and $E \parallel c$ is a result of the anisotropy in the dipole-allowed direct transitions in the vicinity of the VBM at Γ and is not due to transitions from lower-lying VBs. Our conclusions are consistent with other available experimental results. Furthermore, we have predicted the dielectric function for a wide frequency range.

[1] R. Gordon, MRS Bull. **25**, 52 (2000).

[2] M. Batzill and U. Diebold, Prog. Surf. Sci. **79**, 47 (2005).

[3] A. K. Singh, A. Janotti, M. Scheffler, and C. G. Van de Walle, Phys. Rev. Lett. **101**, 055502 (2008).

[4] J. B. Varley, A. Janotti, A. K. Singh, and C. G. Van de Walle, Phys. Rev. B **79**, 245206 (2009).

[5] Z. Ji, Z. He, Y. Song, K. Liu, and Z. Ye, J. Cryst. Growth **259**, 282 (2003).

[6] Z. Ji, L. Zhao, Z. He, Q. Zhou, and C. Chen, Mater. Lett. **60**, 1387 (2006).

[7] J. L. Jacquemin and G. Bordure, J. Phys. Chem. Solids **36**, 1081 (1975).

[8] J. Robertson, J. Phys. C **12**, 4767 (1979).

[9] A. Svane and E. Antoncik, J. Phys. Chem. Solids **48**, 171 (1987).

[10] K. Reimann and M. Steube, Solid State Commun. **105**, 649 (1998).

[11] F. Arlinghaus, J. Phys. Chem. Solids **35**, 931 (1974).

[12] S. F. M. Ph. Barbarat and G. L. Blevennec, J. Mater. Chem. **7**, 2547 (1997).

[13] M. Nagasawa and S. Shionoya, Phys. Rev. Lett. **21**, 1070 (1968).

[14] M. Nagasawa and S. Shionoya, J. Phys. Soc. Jpn. **30**, 158 (1971).

[15] M. Nagasawa and S. Shionoya, Solid State Commun. **7**, 1731 (1969).

[16] S. F. Reddaway and D. A. Wright, Br. J. Appl. Phys. **16** (1965).

[17] R. S. Katiyar, P. Dawson, M. M. Hargreave, and G. R. Wilkinson, J. Phys. C **4**, 2421 (1971).

[18] P. D. Borges, L. M. R. Scolfaro, H. W. L. Alves, and E. F. da Silva, Theor. Chem. Acc. **126**, 39 (2009).

[19] J. Haines and J. M. Léger, Phys. Rev. B **55**, 11144 (1997).

[20] A. A. Bolzan, C. Fong, B. J. Kennedy, and C. J. Howard, Acta Crystallogr. B **53**, 373 (1997).

[21] V. T. Agekyan, Phys. Status Solidi A **43**, 11 (1977).

[22] R. Summitt, J. A. Marley, and N. F. Borrelli, J. Phys. Chem. Solids **25**, 1465 (1964).

[23] R. D. McRoberts, C. G. Fonstad, and D. Hubert, Phys. Rev. B **10**, 5213 (1974).

[24] M. Nagasawa and S. Shionoya, J. Phys. Soc. Jpn. **30**, 1118 (1971).

[25] M. Nagasawa and S. Shionoya, Phys. Lett. **22**, 409 (1966).

[26] D. Fröhlich, R. Kenklies, and R. Helbig, Phys. Rev. Lett. **41**, 1750 (1978).

[27] G. F. Koster, J. O. Dimmock, R. G. Wheeler, and H. Statz, *Properties of the Thirty-two Point Groups* (MIT Press, Cambride, MA, 1963).

[28] V. T. Agekyan, Opt. Spectrosc. **29**, 395 (1970).

[29] V. T. Agekyan, Opt. Spectrosc. **29**, 487 (1970).

[30] Z. Q. Li, Y. L. Yin, X. D. Liu, L. Y. Li, H. Liu, and Q. G. Song, J. Appl. Phys. **106**, 083701 (2009).

[31] F. Thomazi, L. S. Roman, A. F. da Silva, and C. Persson, Phys. Status Solidi C **6**, 2740 (2009).

[32] W. G. Aulbur, L. Jönsson, and J. W. Wilkins, *Solid State Physics: Advances in Research and Applications* (Academic, San Diego, 2000), p. 1.

[33] G. Onida, L. Reining, and A. Rubio, Rev. Mod. Phys. **74**, 601 (2002).

[34] P. Rinke, A. Qteish, J. Neugebauer, and M. Scheffler, Phys. Status Solidi B **245**, 929 (2008).

[35] W. Hanke and L. J. Sham, Phys. Rev. Lett. **43**, 387 (1979).

[36] G. Strinati, Riv Nuovo Cimento **11**, 1 (1988).

[37] P. Hohenberg and W. Kohn, Phys. Rev. **136**, B864 (1964).

[38] W. Kohn and L. J. Sham, Phys. Rev. **140**, A1133 (1965).

[39] G. Kresse and J. Furthmüller, Phys. Rev. B **54**, 11169 (1996).

[40] G. Kresse and J. Furthmüller, Comput. Mater. Sci. **6**, 15 (1996).

[41] M. Shishkin and G. Kresse, Phys. Rev. B **74**, 035101 (2006).

[42] P. E. Blöchl, Phys. Rev. B **50**, 17953 (1994).

[43] G. Kresse and D. Joubert, Phys. Rev. B **59**, 1758 (1999).

[44] D. M. Ceperley and B. J. Alder, Phys. Rev. Lett. **45**, 566 (1980).

[45] J. P. Perdew and A. Zunger, Phys. Rev. B **23**, 5048 (1981).

[46] H. J. Monkhorst and J. D. Pack, Phys. Rev. B **13**, 5188 (1976).

[47] L. Hedin, Phys. Rev. **139**, A796 (1965).

[48] P. Rinke, A. Qteish, J. Neugebauer, C. Freysoldt, and M. Scheffler, New J. Phys. **7**, 126 (2005).

[49] F. Fuchs, J. Furthmüller, F. Bechstedt, M. Shishkin, and G. Kresse, Phys. Rev. B **76**, 115109 (2007).

[50] P. Rinke, M. Winkelnkemper, A. Qteish, D. Bimberg, J. Neugebauer, and M. Scheffler, Phys. Rev. B **77**, 075202 (2008).

[51] A. Schleife, C. Rödl, F. Fuchs, J. Furthmüller, and F. Bechstedt, Phys. Rev. B **80**, 035112 (2009).

[52] F. Bechstedt, F. Fuchs, and G. Kresse, Phys. Status Solidi B **246**, 1877 (2009).

[53] J. Heyd, G. E. Scuseria, and M. Ernzerhof, J. Chem. Phys. **118**, 8207 (2003).

[54] C. Rödl, F. Fuchs, J. Furthmüller, and F. Bechstedt, Phys. Rev. B **79**, 235114 (2009).

[55] S. Albrecht, L. Reining, R. Del Sole, and G. Onida, Phys. Rev. Lett. **80**, 4510 (1998).

[56] S. G. Louie, J. R. Chelikowsky, and M. L. Cohen, Phys. Rev. Lett. **34**, 155 (1975).

[57] F. Fuchs, C. Rödl, A. Schleife, and F. Bechstedt, Phys. Rev. B **78**, 085103 (2008).

[58] F. Bechstedt, R. Del Sole, G. Cappellini, and L. Reining, Solid State Commun. **84**, 765 (1992).

[59] L. X. Benedict, E. L. Shirley, and R. B. Bohn, Phys. Rev. Lett. **80**, 4514 (1998).

[60] M. Rohlfing and S. G. Louie, Phys. Rev. Lett. **81**, 2312 (1998).

[61] W. G. Schmidt, S. Glutsch, P. H. Hahn, and F. Bechstedt, Phys. Rev. B **67**, 085307 (2003).

[62] V. I. Anisimov, J. Zaanen, and O. K. Andersen, Phys. Rev. B **44**, 943 (1991).

[63] S. L. Dudarev, G. A. Botton, S. Y. Savrasov, C. J. Humphreys, and A. P. Sutton, Phys. Rev. B **57**, 1505 (1998).

[64] F. D. Murnaghan, Proc. Natl. Acad. Sci. USA **30**, 244 (1944).

[65] J. B. Varley, A. Janotti, and C. G. Van de Walle, Phys. Rev. B **81**, 245216 (2010).

[66] N. I. Medvedeva, V. P. Zhukov, M. Y. Khodos, and V. A. Gubanov, Phys. Status Solidi B **160**, 517 (1990).

[67] J.-M. Themlin, M. Chtaïb, L. Henrard, P. Lambin, J. Darville, and J.-M. Gilles, Phys. Rev. B **46**, 2460 (1992).

[68] T. Nagata, O. Bierwagen, M. E. White, M.-Y. Tsai, and J. S. Speck, J. Appl. Phys. **107**, 033707 (2010).

[69] K. J. Button, C. G. Fonstad, and W. Dreybrodt, Phys. Rev. B **4**, 4539 (1971).

[70] D. Hobbs, G. Kresse, and J. Hafner, Phys. Rev. B **62**, 11556 (2000).

[71] J. M. Themlin, R. Sporken, J. Darville, R. Caudano, J. M. Gilles, and R. L. Johnson, Phys. Rev. B **42**, 11914 (1990).

[72] A. Schleife, C. Rödl, F. Fuchs, J. Furthmüller, F. Bechstedt, P. H. Jefferson, T. D. Veal, C. F. McConville, L. F. J. Piper, A. DeMasi, K. E. Smith, H. Lösch, R. Goldhahn, C. Cobet, J. Zúñiga-Pérez, and V. Muñoz-Sanjosé, J. Korean Phys. Soc. **53**, 2811 (2008).

[73] P. D. C. King, T. D. Veal, A. Schleife, J. Zúñiga-Pérez, B. Martel, P. H. Jefferson, F. Fuchs, V. Muñoz-Sanjosé, F. Bechstedt, and C. F. McConville, Phys. Rev. B **79**, 205205 (2009).

[74] M. Rohlfing, P. Krüger, and J. Pollmann, Phys. Rev. Lett. **75**, 3489 (1995).

[75] M. Rohlfing, P. Krüger, and J. Pollmann, Phys. Rev. B **57**, 6485 (1998).

[76] A. Fleszar and W. Hanke, Phys. Rev. B **71**, 045207 (2005).

[77] T. Miyake, P. Zhang, M. L. Cohen, and S. G. Louie, Phys. Rev. B **74**, 245213 (2006).

[78] P. L. Gobby and G. J. Lapeyre, in *Physics of Semiconductors*, edited by F. G. Fumi, Proc. XIII Intern. Conf. (1976), p. 150.

[79] R. J. Elliott, Phys. Rev. **108**, 1384 (1957).

[80] C. Schweitzer, K. Reimann, and M. Steube, Solid State Commun. **110**, 697 (1999).

[81] F. Bechstedt, K. Seino, P. H. Hahn, and W. G. Schmidt, Phys. Rev. B **72**, 245114 (2005).

[82] H. J. van Daal, J. Appl. Phys. **39**, 4467 (1968).

[83] Z. M. Jarzebski and J. P. Morton, J. Electrochem. Soc. **123**, 333C (1976).

[84] A. Schleife, C. Rödl, F. Fuchs, J. Furthmüller, and F. Bechstedt, Appl. Phys. Lett. **91**, 241915 (2007).

[85] M. Gajdoš, K. Hummer, G. Kresse, J. Furthmüller, and F. Bechstedt, Phys. Rev. B **73**, 045112 (2006).

[86] A. Schleife, F. Fuchs, C. Rödl, J. Furthmüller, and F. Bechstedt, Phys. Status Solidi B **246**, 2150 (2009).

[87] G. Sanon, R. Rup, and A. Mansingh, Phys. Rev. B **44**, 5672 (1991).